International Journal of Applied Engineering Research
ISSN 0973-4562 Volume 10, Number 9 (2015) pp. 22011-22022

http://www.ripublication.com

A Complexity Reduction Demodulator For Multi-h CPM With Phase And Symbol Timing Synchronization

Minho Choi [1] **and Wonsik Yoon** [2]

Department of Electrical and Computer Engineering, Ajou University
206 Worldcupro Yeongtonggu Suwon Gyeonggido, 443-749, South Korea
min_ho0616@ajou.ac.kr [1] *wsyoon@ajou.ac.kr* [2]
corresponding author : Wonsik Yoon (wsyoon@ajou. ac. kr)

Abstract

This paper present a demodulator for multi-h CPM which is based on maximum likelihood detection. The optimal demodulator has a drawback to have a lot of matched filters with a trellis of states and branches. In this paper, two complexity reduction techniques are applied and thus we implemented a demodulator that includes only 16 real-valued matched filter, trellis of 64 states and 256 branches. We also implemented phase and symbol timing recovery using the derivative of log-likelihood function. The simulation results show the performance of bit error rate (BER), phase recovery, and symbol timing recovery. The proposed demodulator shows few loss relative to the optimum demodulator for multi-h CPM. Also simulation results show that the phase and symbol timing recovery performs well.

1. Introduction

Continuous phase modulation (CPM) represents a family of non-linear coded modulation schemes characterized by a constant envelop and continuity of the phase [1]. It is a jointly power and bandwidth efficient digital modulation scheme [2]. Due to these characteristics, CPM has been used for telemetry. There are some CPM signals adopted as the IRIG-106 standard for aeronautical telemetry such as FQPSK [3], SOQPSK [4], and PCM/FM. However, as data rate have increased and available bandwidth has decreased, the need for more spectrally efficient modulations has intensified. Recently, multi-h CPM, denoted ARTM CPM, was adopted as part of the IRIG-106 standard [5]. This waveform achieves almost three times the spectral efficiency of PCM/FM. This paper describes a demodulator of multi-h CPM with

phase and symbol timing recovery.

A multi-h CPM detector is based on maximum likelihood detection. The optimal detector requires 128 real-valued matched filters together with a trellis consisting of 512 states and 2048 branches. Thus, the optimal detector has a high complexity. For the complexity reduction, this paper applied the two complexity reducing techniques such as tilted phase [6] and frequency pulse truncation [7, 8]. As a result, the proposed demodulator in this paper only requires 16 real-valued matched filters together with a trellis consisting of 64 states and 256 branches.

In an actual demodulator, phase and symbol timing synchronization is essential. If the synchronization is not implemented in the demodulator, it is difficult to obtain an accurate detection result. First, the role of the phase recovery is to compensate the phase offset. Conceptually, phase recovery is the process of forcing the local oscillators in the detector to oscillate in both phase and frequency of the received signal. Phase recovery presented in this paper is based on the phase-locked loop (PLL). A derivative of the log-likelihood [9] is used to find the phase offset. Second, symbol timing recovery is the process of estimating a clock signal that is aligned in both phase and frequency with the clock of the received data. Symbol timing recovery presented in this paper is also based on the PLL. A derivative of the log-likelihood is used to find the accurate clock position.

This paper is organized as follows. Multi-h CPM detection and complexity reducing techniques are described in Section 2. Phase and symbol timing synchronization are described in Section 3. Performance evaluation is presented in Section 4. Finally, the conclusions of this paper are presented in Section 5.

2. Multi-h CPM detection and Complexity reduction techniques

In multi-h CPM detector design, we use maximum likelihood detection. Furthermore, tilted phase and frequency pulse truncation scheme are used to reduce complexity.

A. Maximum likelihood detection

The complex baseband CPM signal can be represented as [1]

$$s(t;\boldsymbol{\alpha}) = \exp\{ j\phi(t;\boldsymbol{\alpha})\}. \tag{1}$$

Here the phase is the form of pulse train given by

$$\phi(t;\boldsymbol{\alpha}) = 2\pi \sum_i h_i \alpha_i q(t - iT) \tag{2}$$

where α_i denotes an $M-ary$ symbol, T is the symbol time, and $q(t)$ is the phase pulse which is time-integral of frequency pulse with half of area. The parameters of multi-h CPM are summarized in Table 1 [10, 11].

During the k-th symbol interval, $kT \le t \le (k+1)T$, the phase is given by

$$\phi(t;\boldsymbol{\alpha}) = \underbrace{2\pi \sum_{i=k-2}^{k} h_i \alpha_i q(t-iT)}_{\theta(t;\boldsymbol{\alpha}_k)} + \underbrace{\pi \sum_{i=0}^{k-3} h_i \alpha_i}_{\vartheta_{k-3}} \tag{3}$$

where $\boldsymbol{\alpha}_k = \alpha_{k-2}, \alpha_{k-1}, \alpha_k$. The first term $\theta(t;\boldsymbol{\alpha}_k)$ is the phase trajectory of latest two symbols during the interval $kT \le t \le (k+1)T$. The second term ϑ_{k-3} is the cumulative phase which represents the contribution to the carrier phase from all symbols that have worked their way through the frequency pulse and contribute a constant value to the overall phase.

Table 1. Parameters of multi-h CPM

Symbol values	$\alpha_i \in \{-3, -1, +1, +3\}$
Partial response	$L = 3$
Frequency pulse	$g(t) = \begin{cases} \dfrac{1}{2LT}\left[1 - \cos\left(\dfrac{2\pi t}{LT}\right)\right] & 0 \le t \le LT \\ 0 & \text{otherwise} \end{cases}$
Phase pulse	$q(t) = \begin{cases} 0 & t \le 0 \\ \int_0^t g(\tau)d\tau & 0 \le t \le LT \\ 1/2 & t \ge LT \end{cases}$
Modulation index	$h_i \in \left\{\dfrac{4}{16}, \dfrac{5}{16}\right\}$

When the transmitted signal is represented by equation (1), the received signal of multi-h CPM is given by [10]

$$r(t) = \exp\{\phi(t;\boldsymbol{\alpha})\} + \omega(t) \tag{4}$$

where $\omega(t)$ is zero-mean Gaussian noise with power spectral density $N_0/2$ W/Hz. The recursive expression for maximum likelihood detector output is given by

$$\mathrm{Re}\left[\int_0^{(k+1)T} r(t)e^{-j\phi(t;\boldsymbol{\alpha})}dt\right] = \mathrm{Re}\left[\int_0^{kT} r(t)e^{-j\phi(t;\boldsymbol{\alpha})}dt\right] + \mathrm{Re}\left[\int_{kT}^{(k+1)T} r(t)e^{-j\phi(t;\boldsymbol{\alpha})}dt\right]. \tag{5}$$

By using the equation (3), we can express the last term in equation (5) as

$$\mathrm{Re}\left[\int_k^{(k+1)T} r(t)e^{-j\phi(t;\boldsymbol{\alpha})}dt\right] = \mathrm{Re}\left[e^{-j\vartheta_{k-3}}\int_0^{kT} r(t)e^{-j\phi(t;\boldsymbol{\alpha})}dt\right]. \tag{6}$$

The optimal detector requires $M^L = 64$ matched filters, $pM^{L-1} = 512$ trellis states, and $pM^L = 2048$ branches where $p = 32$ indicates the possible cumulative phase values.

B. Complexity reduction techniques

First, we apply one of the complexity-reducing techniques which is called as "tilted phase". This method exploits the property that available trellis states according to odd or even symbol are restricted. The possible cumulative phases are summarized in Table 2. For this method, we use the data symbols $U_i = (\alpha_i + M - 1)/2$ in place of the original data α_i when defining the cumulative phase. Therefore, we have

$$\vartheta_{k-3} = \pi \sum_{i=0}^{k-3} h_i \alpha_i = \nu_{k-3} + \underbrace{2\pi \sum_{i=0}^{k-3} h_i U_i}_{\theta_{k-3}} \tag{7}$$

where the data-independent phase tilt is defined as $\nu_i = \nu_{i-1} - \pi h_i (M-1)$. By using equation (7), the number of trellis states can be reduced from $pM^{L-1} = 512$ to $p'M^{L-1} = 256$ where $p' = 16$ indicates only half the number of cumulative phases. The number of branches are also reduced from $pM^L = 2048$ to $p'M^L = 1024$. The tilted phase technique can achieve the same bit error rate as optimal detection since the tilted phase technique is lossless in detection efficiency.

Table 2. The cumulative phase in the odd and even intervals of multi-h CPM

Symbol intervals	Odd intervals	Even intervals
Cumulative phase states	$\vartheta_{k-L} \in \left\{ \frac{\pi}{16}, \frac{3\pi}{16}, \frac{5\pi}{16}, \cdots, \frac{31\pi}{16} \right\}$	$\vartheta_{k-L-1} \in \left\{ 0, \frac{2\pi}{16}, \frac{4\pi}{16}, \cdots, \frac{30\pi}{16} \right\}$

Another complexity-reducing technique is "frequency pulse truncation". This technique demodulates phase pulse based on approximating the partial response to full response. In pulse truncation it only compares the correlation of frequency pulse and phase pulse within one symbol from $0.5T$ to $2.5T$. By approximating the frequency pulse with a length-$2T$ pulse, the phase trajectory $\theta(t;\alpha_{k-2},\alpha_{k-1},\alpha_k)$ can be replaced by a new phase trajectory $\tilde{\theta}(t;\alpha_{k-1},\alpha_k)$ [10]. As a consequence, the metric update equation becomes

$$\lambda(k) = \lambda(k-1) + \underbrace{\mathrm{Re}\left[e^{-j\vartheta_{k-2}} \int_{(k+1/2)T}^{(k+3/2)T} r(t) e^{-j\tilde{\theta}(t;\alpha_{k-1},\alpha_k)} dt \right]}_{z_k(\vartheta_{k-2},\alpha_{k-1},\alpha_k)} \tag{8}$$

where $\tilde{\theta}(t;\alpha_{k-1},\alpha_k) = 2\pi \sum_{i=k-1}^{k} h_i \alpha_i q_{PT}(t - iT)$. The truncated phase pulse is given by

$$q_{PT}(t)=\begin{cases}0 & t\le T/2\\ q(t) & T/2\le t\le 5T/2.\\ 1/2 & t\ge 5T/2\end{cases} \tag{9}$$

Tilted phase equation is defined newly by pulse truncation as

$$\vartheta_{k-2}=\pi\sum_{i=0}^{k-2}h_i\alpha_i=\nu_{k-2}+\underbrace{2\pi\sum_{i=0}^{k-2}h_iU_i}_{\theta_{k-2}} \tag{10}$$

When we use the pulse truncation with the detector which applies the tilted phase, the length of frequency pulse $L=2$ is reduced to $L'=1$. Therefore, the number of matched filter is reduced to $M^{L'}=16$. The number of trellis states and branches also reduced to $p'M^{L'-1}=64$ and $p'M^{L'}=256$, respectively.

C. Implementation of the detector

We implemented a detector of multi-h CPM using the equation (8) and (10). The structure of detector is based on equation (8). The trellis diagram of Viterbi algorithm is based on equation (10). The block diagram of the detector for multi-h CPM is illustrated in Fig. 1.

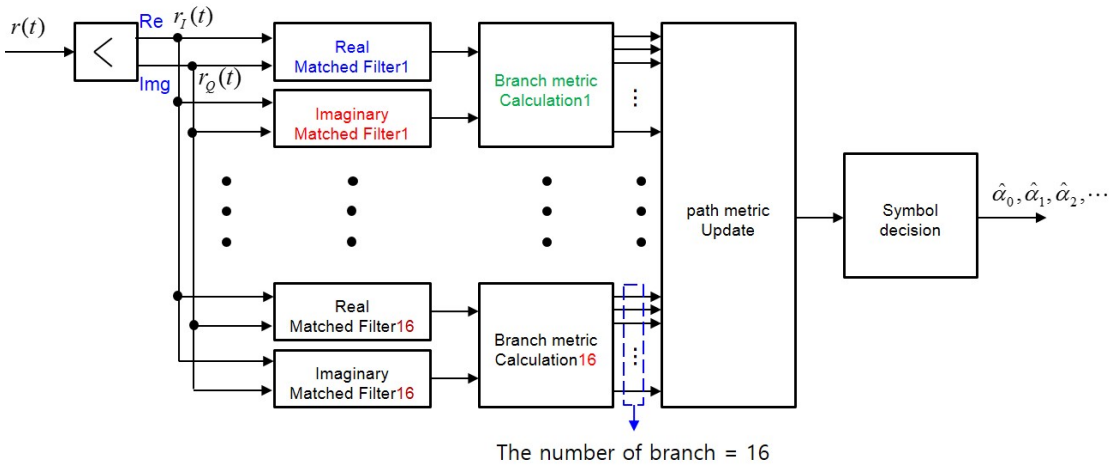

Figure1. Block diagram of detector for multi-h CPM

The actual detector is implemented by dividing a complex plane into in-phase and quadrature parts. $r_I(t)$ is the in-phase received signal and $r_Q(t)$ is the quadrature received signal. By using the Euler's theorem, the branch increment term $Z_k(\vartheta_{k-2},\alpha_{k-1},\alpha_k)$ in equation (8) can be rewritten as [12]

$$Z_k(\vartheta_{k-2},\alpha_{k-1},\alpha_k)=\cos(\vartheta_{k-2})\left[\int_{(k+1/2)T}^{(k+3/2)T} r_I(t)\cos(\tilde{\theta}(t;\alpha_{k-1},\alpha_k))+r_Q(t)\sin(\tilde{\theta}(t;\alpha_{k-1},\alpha_k))dt\right] \\ +\sin(\vartheta_{k-2})\left[\int_{(k+1/2)T}^{(k+3/2)T} r_Q(t)\cos(\tilde{\theta}(t;\alpha_{k-1},\alpha_k))-r_I(t)\sin(\tilde{\theta}(t;\alpha_{k-1},\alpha_k))dt\right] \quad (11)$$

where the first integration term is the in-phase matched filter and the second integration term is the quadrature matched filter. The branch metric is calculated by using the in-phase and quadrature matched filters output, and cumulative phases. The calculated branch metrics are used for trellis diagram in the path metric update. Trellis diagrams of the proposed detector are shown in Fig. 2 and Fig. 3.

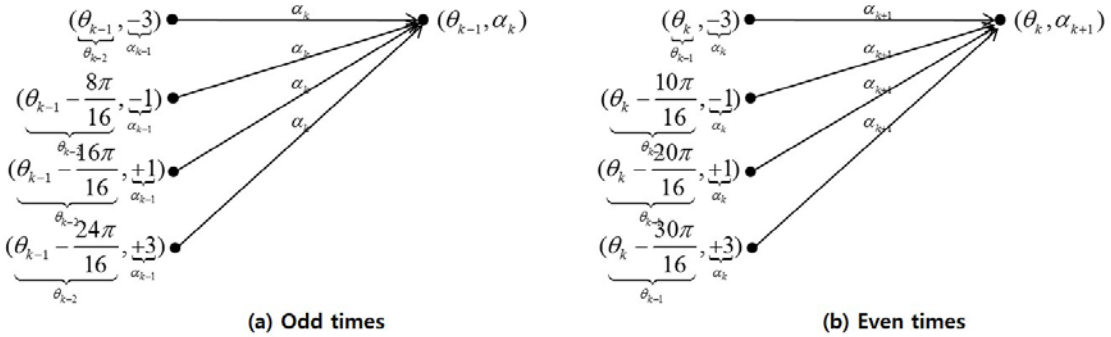

Figure 2. Trellis diagram of the proposed detector for the evaluating survival path

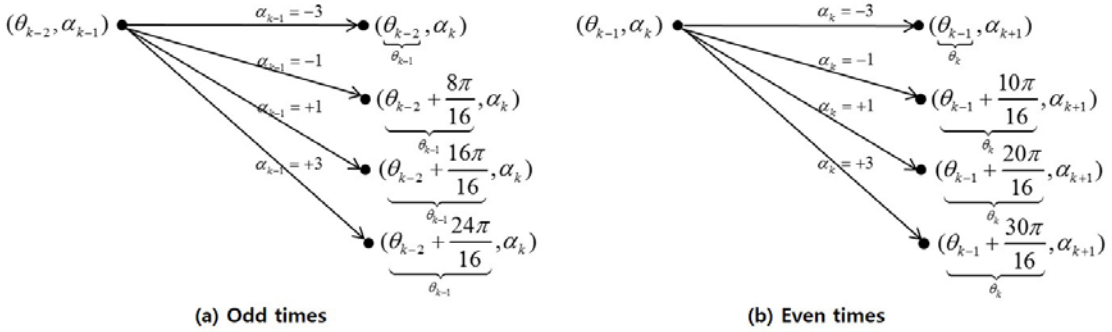

Figure 3. Trellis diagram of the proposed detector for the updating accumulated distance

We can use the tilted phase if we construct a time varying trellis with different sections for odd and even. The labels above each branch show the input symbol for the given branch using tilted phase. There are two trellis diagrams for the survival path and accumulated distances. Each states evaluates the four branch metric candidates in Fig. 2 and updates the accumulated distances according to Fig. 3. The survival path is selected to the largest branch that is the combined value of the new branch increment and accumulated distance. Finally, the detector determines the symbols by the survival path in Viterbi algorithm.

3. Phase and Symbol timing synchronization

The proposed demodulator for multi-h CPM contains phase and symbol timing synchronization. The simplified block diagram of demodulator for multi-h CPM is illustrated in Fig. 4. The architecture consists of three major blocks: multi-h CPM detector, phase recovery, and symbol timing recovery. These blocks of the phase and symbol timing recovery are detailed in the following subsections.

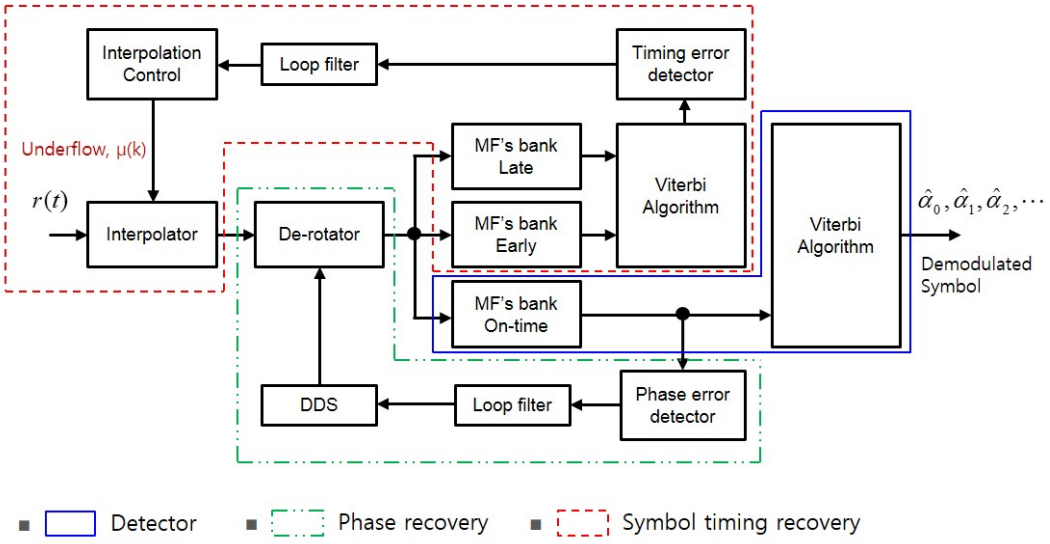

Figure 4. Block diagram of demodulator for multi-h CPM

A. Phase recovery

The carrier phase synchronization must remove the phase shifts and track the remaining phase. Phase recovery is comprised of phase error detector, phase error estimation, and phase error correction.

First, the phase error detector calculates the phase error signal value. The estimation of the phase offset $\tilde{\phi}_0$ is the value of the carrier phase that maximizes the logarithm of $Z_k(\vartheta_{k-2}, \alpha_{k-1}, \alpha_k)$ in equation (8), which is the log-likelihood function. In order to recover the phase offset, we need to take the partial derivative of the log-likelihood function. The phase error signal $e_{\tilde{\phi}_0}[k]$ is given by [9]

$$e_{\tilde{\phi}_0}[k] = \frac{\partial}{\partial \phi_0} \log\left\{Z_k(r \mid \tilde{\phi}_0)\right\} = \mathrm{Im}\left\{e^{-j\tilde{\phi}_0} \boldsymbol{M}_k(\alpha_k) e^{-j\vartheta_{k-2}}\right\} \tag{12}$$

where $Z_k(r \mid \tilde{\phi}_0)$ is the branch increment including phase error and $\boldsymbol{M}_k(\alpha_k)$ is the matched filter output. Here, phase error signal forces to zero. Because equation (12) does not adequate on implementation, it can be rewritten as

$$e_{\tilde{\phi}_0}[k] = e^{-j\tilde{\phi}_0}\begin{bmatrix} \cos(\vartheta_{k-2})\int_{(k+1/2)T}^{(k+3/2)T} r_Q(t)\cos(\tilde{\theta}(t;\alpha_{k-1},\alpha_k)) - r_I(t)\sin(\tilde{\theta}(t;\alpha_{k-1},\alpha_k))dt \\ -\sin(\vartheta_{k-2})\int_{(k+1/2)T}^{(k+3/2)T} r_I(t)\cos(\tilde{\theta}(t;\alpha_{k-1},\alpha_k)) + r_Q(t)\sin(\tilde{\theta}(t;\alpha_{k-1},\alpha_k))dt \end{bmatrix} \quad (13)$$

Second, the phase estimation generates the angle corresponding to the estimated phase error using the phase error signal produced by the timing error detector through loop filter and DDS (Direct Digital Synthesizer). Here, loop filter is designed by second-order PLL [9, 13]. The phase error correction compensates the phase offset using the DDS outputs in De-rotator.

B. Symbol timing recovery

The optimum sampling instant for the in-phase and quadrature matched filter outputs is the center of the each symbol duration. Timing recovery is comprised of timing error detection, timing error estimation, and interpolator.

First, the timing error detector calculates the timing error signal value. The estimation of timing delay $\tilde{\tau}$ is the value of the symbol timing delay that maximizes the logarithm of $Z_k(\vartheta_{k-2},\alpha_{k-1},\alpha_k)$. In order to find $\tilde{\tau}$ we need to take the partial derivative of the log-likelihood function. Thus, the timing error signal $e_{\tilde{\tau}}[k]$ is given by [9]

$$e_{\tilde{\tau}}[k] = \frac{\partial}{\partial\tilde{\tau}}\log\{Z(r\mid\tilde{\tau})\} = \mathrm{Re}\left\{e^{-j\tilde{\phi}_0}\mathbf{Y}_k(\alpha_k,\tilde{\tau})e^{-j\vartheta_{k-2}}\right\} \quad (14)$$

where $\mathbf{Y}_k(\cdot)$ is the partial derivative of the matched filter output $\mathbf{M}_k(\alpha_k)$ with respect to $\tilde{\tau}$. $\mathbf{Y}_k(\cdot)$ can be approximated with the difference between a late and an early matched filter output samples.

Second, the timing error estimation includes a loop filter and interpolation control. The purpose of the loop filter is to provide an adjusting value to the interpolation control based on the timing error signal. In this paper, the transfer function of the loop filter is implemented by $F(s)=k$. This loop filter produces a first-order PLL, where $K_p=1$ and $K_I=-0.0026$. The purpose of the interpolation control is to provide the interpolator with the k-th base point index $m(k)$ and the k-th fractional interval $\mu(k)$. The interpolation control [13, ch8] is implemented by a modulo-1 decrementing counter. In general the counter value satisfies the recursion

$$\eta(n+1) = \left(\eta(n) - 1/N - v(n)\right) \bmod 1 \quad (15)$$

where $v(n)$ is the loop filter output. If the value of $\eta(n+1)$ is negative, the underflows occur in the sample times of the desired inter polant. When the decrementing counter underflows, n is the base point index $m(k)$, and the value of

counter becomes

$$\eta\left(m(k)+1\right)=1+\eta\left(m(k)\right)-1/N-v(n) \tag{16}$$

When the counter underflows, it leads to the relationship

$$\frac{\mu\left(m(k)\right)}{\eta\left(m(k)\right)}=\frac{1-\mu\left(m(k)\right)}{1-\eta\left(m(k)+1\right)} \tag{17}$$

Solving for $\mu(k)$ by using the above equation, we obtain

$$\mu\left(m(k)\right)=\frac{\eta\left(m(k)\right)}{\frac{1}{N}+v(n)} \tag{18}$$

Third, the role of the interpolator is to compute samples in the desired time instants, so that the matched filter outputs are aligned with the center of the each symbol duration. The received signal $r(t)$ is sampled by the ADC at a rate $1/T_s$. The equation for interpolation can be expressed as (19) for a desired sample [13, ch8] at $t=kT$.

$$r(kT)=r(nT_s)+\mu(k)\left[r\left((n+1)T_s\right)-r(nT_s)\right] \tag{19}$$

This sample corresponds to the on-time interpolated sequence that will produce the aligned matched filter outputs. We also need an early and a late matched filter outputs in order to approximate the derivative $\mathbf{Y}_k(\cdot)$. The early interpolated samples are computed by

$$r\left((k-1)T\right)=r\left((n-1)T_s\right)+\mu(k)\left[r(nT_s)-r\left((n-1)T_s\right)\right] \tag{20}$$

and the late interpolated samples are computed by

$$r\left((k+1)T\right)=r\left((n+1)T_s\right)+\mu(k)\left[r\left((n+2)T_s\right)-r\left((n+1)T_s\right)\right] \tag{21}$$

4. Performance Evaluation

The performance of the described demodulator was simulated for multi-h CPM. The results of these simulations are plotted in Fig. 5. We compared the theoretic BER curve with the proposed demodulator BER curve. In fact, the performance between the theoretic and proposed demodulator is relatively similar as shown in Fig. 5. The proposed demodulator loses about 0.8 dB in terms of BER performance compared to

the theory.

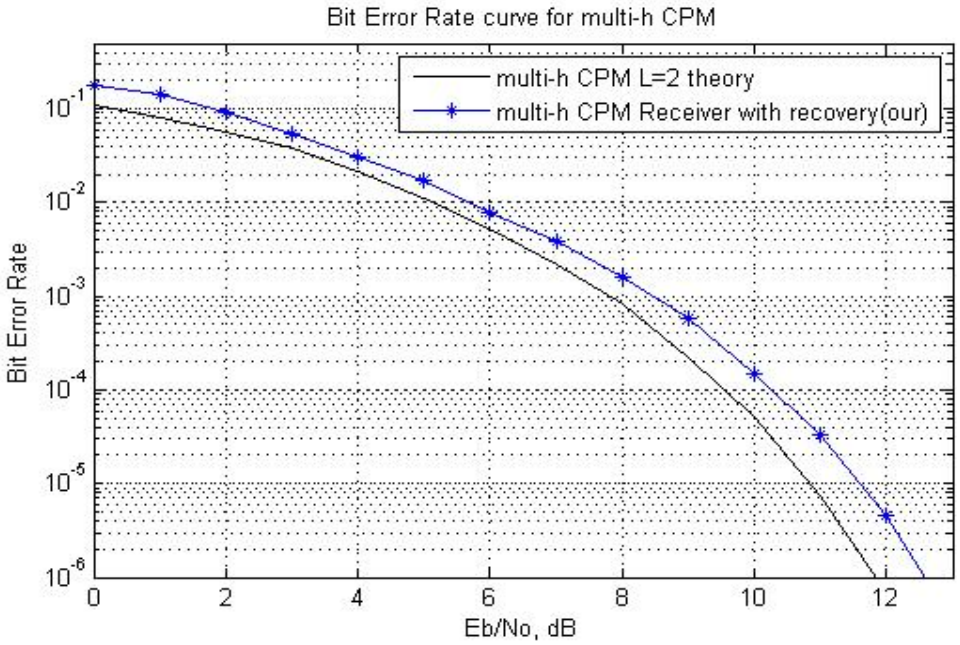

Figure 5. Bit error rate for multi-h CPM demodulator

Fig. 6 shows the convergence curves of the phase offset compensation when the phase offsets are 7°, 10°, and -5°, respectively. The phase error signals converge at about 2000 symbols. As a result, one can see that the phase recovery performs well.

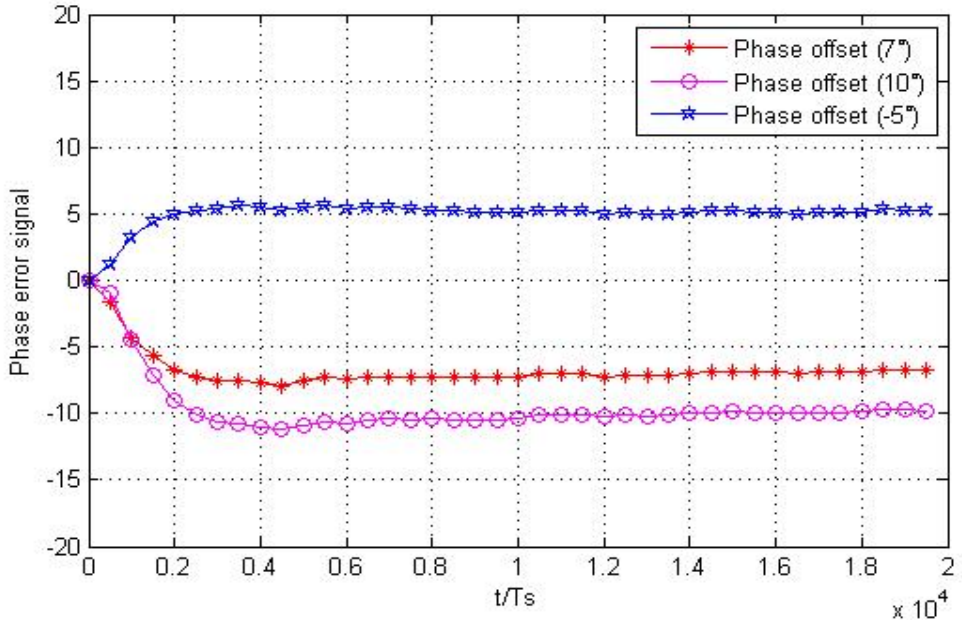

Figure 6. Convergence curve of phase recovery

Fig. 7 shows the convergence curves of the fractional interval when the symbol timing delays are -2.8 sample, -1.3 sample, and 0.5 sample, respectively. The plot of the fractional interval converges at about 2500 symbols. In the process of the fractional interval convergence, the PLL has to find the right clock signal for the desired matched filter output. From Fig. 7, one can see that the symbol timing recovery performs well.

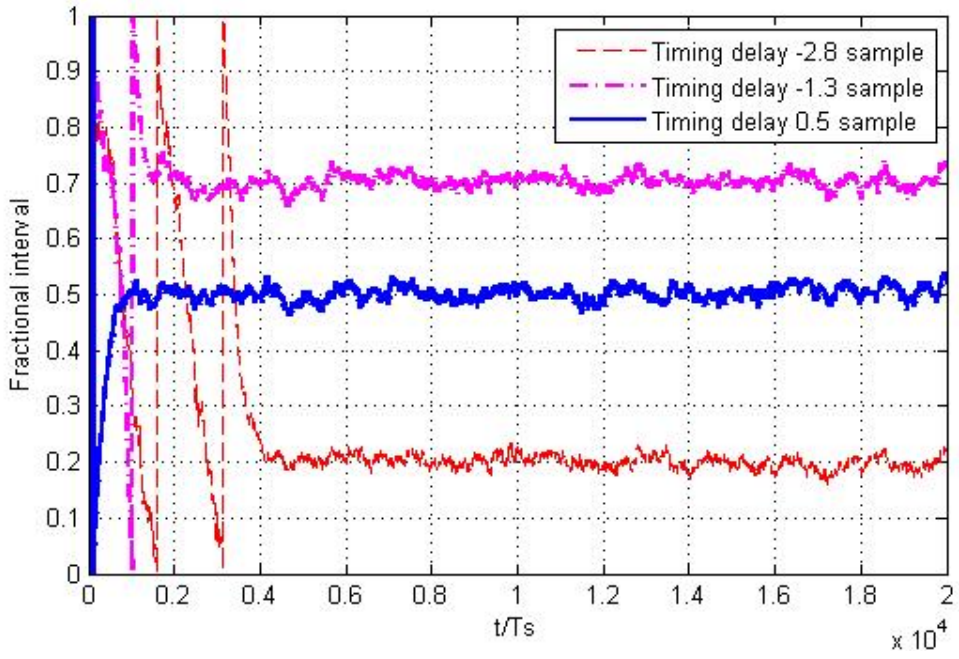

Figure 7. Convergence curve of symbol timing recovery

5. Conclusion

In this paper, we implement a demodulator of the multi-h CPM and show its performance. The complexity reduction techniques reduce the number of trellis states to about 10 percent with about 0.8 dB performance losses. Note that the implementation is a very successful complexity reduction demodulator for multi-h CPM using the frequency pulse truncation and tilted phase. The proposed demodulator also contains phase recovery and symbol timing recovery. Simulation results show that the recovery sub blocks perform well.

Acknowledgements

Following are results of a study on the "Leades INdustry-university cooperation" Project, supported by the Ministry of Education, Science & Technology (MEST).

References

[1] J. B. Anderson, T. Aulin, and C. E. Sundberg, *Digital Phase Modulation.* New York, Plenum Press, 1986

[2] C. H. Kuo, and K. M. Chugg, "On the bandwidth efficiency of CPM signals, " *IEEE MILCOM,* vol 1, 2004.

[3] W. Gao, and K. Feher, "FQPSK: A bandwidth and RF power efficient technology for telemetry application, " in *Proceedings of the International Telemetering Conference*, Las Vegas, NV, pp 480-488, Oct. 1997.

[4] T. Hill, "An enhanced, constant envelope, interoperable shaped offset QPSK (SOQPSK) waveform for improved spectral efficiency, " in *Proceedings of the International Telemetering Conference*, San Diago, CA, pp 127-136, Oct. 2000.

[5] T. Hill, "Performance of SOQPSK and multi-h CPM in the presence of adjacent channel interference, " in *Proceedings of the International Telemetering Conference*, Las Vegas, NV, pp 255-263, Oct. 2001.

[6] B. E. Rimoldi, "A decomposition approach to CPM, " *IEEE Transactions on Information Theory*, pp 260-270, Mar. 1988.

[7] A. Svensson, C. E. Sundberg, and T. Aulin, ″Viterbi detectors with reduced complexity for partial response continuous phase modulation, " in *Proceedings of the National Telecommunications Conference*, New Orleans, LA, 1981.

[8] A. Svensson, C. E. Sundberg, and T. Aulin, "Class of reduced-complexity Viterbi detectors for partial response continuous phase modulation" *IEEE Transactions on Communications*, vol. 32, pp. 1079-1087, Oct. 1984.

[9] G. R. Zanabria, “A hardware implementation of a coherent SOQPSK-TG demodulator for FEC applications, ” M. S. thesis, Kansas, 2011.

[10] E. Perrins, and M. Rice, ″Reduced-complexity detector for multi-h CPM in aeronautical telemetry, ” *IEEE Transactions on Aerospace and Electronic System,* vol. 43, pp. 286-300, Jan. 2007.

[11] D. Kumaraswamy, ″Simplified detection techniques for serially concatenated coded continuous phase modulation, ” M. S. thesis, Kansas, 2007.

[12] A. B. Bridger, ″Increasing the spectral efficiency of continuous phase modulation applied to digital microwave radio: a resource efficient FPGA receiver implementation, ” M. S. thesis, Massey, 2009.

[13] M. Rice, *Digital Communications: A Discrete-Time Approach.* New York: Prentice Hall, 2009.